

Generalized Heralded Generation of Non-Gaussian States Using an Optical Parametric Amplifier

Xiao-Xi Yao, Bo Zhang and Yusuf Turek*
School of Physics, Liaoning University, Shenyang, Liaoning 110036, China

The heralded optical parametric amplifier (OPA) has emerged as a promising tool for quantum state engineering. However, its potential has been limited to coherent state inputs. Here, we introduce a generalized heralded OPA protocol that unlocks a vastly expanded class of quantum phenomena by accepting arbitrary non-classical inputs. With a squeezed vacuum input, the setup functions as an integrated two-photon subtractor, deterministically generating high-fidelity, larger-amplitude squeezed Schrödinger cat states—an operation previously requiring complex, discrete setups. Furthermore, when fed a small-amplitude SC state, the protocol acts as a non-Gaussianity amplifier, distilling it into high-purity approximations of key quantum resources like specific photon-number superpositions. This work transforms the OPA from a specialized source into a versatile and practical platform for advanced quantum state engineering, enabling the generation of a wide array of non-Gaussian states from a single, integrated setup.

I. INTRODUCTION

Non-Gaussian (nG) states [1, 2] are indispensable resources in quantum information science. By going beyond the limitations of the Gaussian framework, they are crucial for achieving a continuous-variable (CV) quantum computational advantage [3–7], for enabling fault-tolerant quantum computation with encoded qubits [8], and for enhancing quantum metrology [9, 10]. nG states are typically characterized by the negativity of their Wigner functions and the presence of higher-order quantum correlations. Among the most extensively studied nG states are photon-added coherent states [11], squeezed Fock states [12], and Schrödinger cat (SC) states [13]. However, the generation of high-quality nG states remains experimentally challenging due to practical limitations of existing methods.

Traditional approaches for producing nG states generally fall into two categories: nonlinear optical processes [14, 15] and conditional measurements such as photon addition/subtraction [16], photon catalysis [17] and weak value amplification technique [18, 19]. While nonlinear optical schemes can, in principle, deterministically generate nG states, their implementation is severely constrained by the weakness of optical nonlinearities. In addition, such schemes often suffer from poor scalability and strong susceptibility to losses, which limit their practical feasibility. In recent years, substantial efforts have been devoted to generating nG states from Gaussian states via conditional measurements. The key idea is to realize effective nG operations—such as photon addition or subtraction [20–25] by beam splitters. For example, subtracting a single photon from a squeezed vacuum (SV) state can produce an odd SC state [26]; however, the resulting SC states usually possess small coherent amplitudes ($\alpha < 1.2$) and therefore exhibit only weak non-Gaussianity. In many quantum technologies, stronger nG

resources are essential to achieve genuine performance advantages [4, 27–30]. Another well-known example is the generation of SC states with arbitrary amplitudes ($\alpha = \sqrt{n}$ for $n \geq 3$) by performing conditional measurements on Fock states $|n\rangle$ [31] and two-mode Gaussian states [32]. However, producing high-purity n photon number states and its effective detection remains technically demanding, which makes the practical implementation of this approach challenging. Moreover, most existing models are restricted to generating only a specific type of nG state, lacking the flexibility and universality needed for a scalable quantum technology.

The preparation of nonclassical light relies predominantly on nonlinear media, with second- and third-order nonlinearities being particularly important. Among second-order nonlinear devices, the optical parametric amplifier (OPA) stands as a fundamental component for generating a variety of quantum states. Its versatility allows for the effective generation of both two-mode and single-mode SV states under non-degenerate and degenerate operational phase matching conditions, respectively. A recent seminal study by Shringarpure and Franson [33] further demonstrated the OPA’s power in a heralded configuration. In their scheme, injecting a coherent state and a single photon into the signal and idler modes, respectively, creates entanglement between them. The subsequent detection of a single photon in the output idler mode then heralds the generation of useful nG states at the signal output, such as single-photon-added coherent (SPAC) and displaced single-photon states. While seminal, this scheme was confined to a single class of input states (coherent states), leaving open a fundamental question: does the true power of the heralded OPA lie in its ability to process already non-classical states, thereby acting as a nonlinear quantum processor rather than just a state generator?

In this work, we affirmatively answer this question by generalizing the heralded OPA protocol to accommodate arbitrary non-classical signal states. We specifically demonstrate that using a SV state as the input

* Corresponding author: yusufu1984@hotmail.com

enables the deterministic engineering of a high-fidelity, larger-amplitude squeezed SC state with a coherent amplitude of approximately $\alpha \approx 1.4$ —an operation functionally equivalent to an integrated two-photon subtraction. Furthermore, we show that when the input is already a nG state, such as a small-amplitude SC state, our protocol acts as a powerful amplifier of non-Gaussianity. By tuning the amplitude gain g , we can significantly enhance the Wigner negativity of both even and odd SC states, distilling them into high-purity approximations of key quantum resources. The significance of our generalized system is threefold: it is (1) scalable, as it leverages integrated optics; (2) practical, offering high success probabilities commensurate with other heralding schemes; and (3) versatile, capable of generating a wide class of high-quality nG states from a single setup. This establishes our generalized heralded OPA protocol as a promising and unified platform for advancing quantum optics and quantum information processing.

The structure of this paper is organized as follows. In Sec. II, we review the protocol for nG state generation based on the OPA. In Sec. III and IV, we discuss the cases of a SV input and a small-amplitude SC state input, respectively. In these sections, we analyze the output states through their Wigner functions and Wigner-negative volumes to quantitatively characterize their nG features. In Sec. V, we briefly discuss the effects of photon loss on the nonclassicality of generated states. Finally, we present a discussion and summarize our work in Sec. VI.

II. MODEL SETUP

Our work is motivated by Ref. [33]; a schematic of our setup is shown in Fig. 1. In this scheme the action of OPA plays an essential role. We therefore begin with a brief introduction to the OPA’s function. The Hamiltonian of an OPA can be described by the three-wave mixing device [34, 35]

$$H = \hbar\omega_s a^\dagger a + \hbar\omega_i b^\dagger b + \hbar\omega_p c^\dagger c + i\hbar\chi^{(2)} (abc^\dagger - a^\dagger b^\dagger c), \quad (1)$$

where a , b , and c are the annihilation operators of the signal, idler, and pump with frequencies ω_s , ω_i , and ω_p , respectively, and $\chi^{(2)}$ is the coupling strength, determined by the second-order nonlinear susceptibility of the BBO crystal. Assuming the pump field is a high-amplitude coherent state $|\gamma e^{-i\omega_p}\rangle$ and can therefore be treated classically, we rewrite the Hamiltonian in the interaction picture with $\omega_p = \omega_s + \omega_i$ as

$$H_I = i\hbar (\xi^* ab - \xi a^\dagger b^\dagger), \quad (2)$$

where $\xi = \gamma\chi^{(2)}$. The unitary operator corresponding to this interaction Hamiltonian reads

$$U_I(t) = e^{-iH_I t/\hbar} = \exp [\tau^* ab - \tau a^\dagger b^\dagger] \equiv S(\tau), \quad \tau = \varrho e^{i\delta}. \quad (3)$$

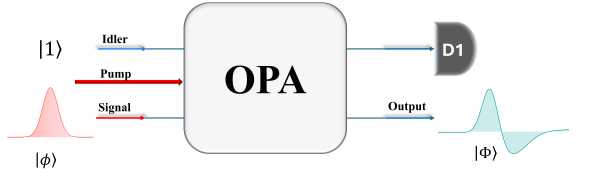


Figure 1. Schematic of non-Gaussian state generation using an OPA. Specific states $|\phi\rangle$ —such as squeezed vacuum and small-amplitude Schrödinger cat (SC) states— are injected into the signal mode, while a single photon is input into the idler mode of the OPA. A single-photon detection at the idler output port heralds the generation of a non-Gaussian quantum state $|\Phi\rangle$ at the signal output. The characteristics of the output state can be controlled by adjusting the gain of the amplifier.

This is a two-mode squeezing operator with a complex squeezing parameter τ . By using the OPA, in the Heisenberg picture, the annihilation operator of the signal mode undergoes the transformation

$$\begin{aligned} a_{out} &= S^\dagger(\tau) a S(\tau) = ga - b^\dagger e^{i\delta} \sqrt{g^2 - 1} \\ &= ga + L^\dagger, \end{aligned} \quad (4)$$

where $g = \cosh \varrho$ and $L = -b^\dagger e^{i\delta} \sinh \varrho$ is the noise operator and one usually assumes that $\langle L^\dagger \rangle = 0$. Eq. (4) represents the physical requirement of an optical amplifier in terms of input-optput relation [36]. By passing in this kind of nonlinear medium, the mean photon number of input signal beam increases with increasing the parameter ϱ , and we refer to g as the amplitude gain. This is a key reason why the second-order nonlinear medium described by the interaction Hamiltonian H_I is termed an OPA. If the signal and idler modes are initially in the vacuum state, $|0\rangle_a |0\rangle_b$, the OPA transforms them into a two-mode squeezed vacuum (TMSV) state:

$$\begin{aligned} |\tau\rangle &= S(\tau) |0, 0\rangle = \exp [\tau^* ab - \tau a^\dagger b^\dagger] |0\rangle_a |0\rangle_b \\ &= \frac{1}{\cosh \varrho} \sum_{n=0}^{\infty} (-e^{i\delta} \tanh \varrho)^n |n, n\rangle. \end{aligned} \quad (5)$$

This state is not a product of two single-mode SV states but is instead an entangled state exhibiting strong correlations between the two modes. Note that for a TMSV state, the reduced density matrix of either mode is a classical state—specifically, a thermal state:

$$\rho_{th} = (1 - \lambda_r) \sum_{n=0}^{\infty} \lambda_r^n |n\rangle \langle n| = \sum_{n=0}^{\infty} \frac{\langle n \rangle_{th}^n}{(1 + \langle n \rangle_{th})^{n+1}} |n\rangle \langle n|. \quad (6)$$

Here, $\lambda_r = \tanh r$ and $\langle n \rangle_{th} = \text{Tr} (a^\dagger a \rho_{th}) = \text{Tr} (b^\dagger b \rho_{th})$ represents the average number of excitations. The thermal state, which describes each mode of the TMSV state, has a Gaussian profile in phase space. Furthermore, in the degenerate case (i.e., $a = b$) the two-mode squeezed operator $S(\tau)$ becomes the conventional squeezed operator as $\exp[\tau^* a^2 - \tau a^{\dagger 2}]$. In this case, if the initial signal state is prepared in vacuum and coherent states, the

output state gives SV and squeezed coherent states, respectively.

However, in Ref. [33] the authors introduced the nG state generation proposal based on OPA with conditional measurement carried out on the idler mode. As shown in schematic, Fig. 1, if the signal mode is prepared in coherent state and idler mode contains single-photon, then some typical nG states can be generated at signal output if a single-photon heralded in output idler mode.

If we consider the general case, the conditional state generation process via OPA can be described as below:

(i) The signal mode input is prepared in single mode radiation field state $|\phi\rangle$ while the idler mode contains single-photon.

(ii) The initial composite state $|\phi\rangle_s|1\rangle_i$ passes through OPA and is transformed into $S|\phi\rangle_s|1\rangle_i$. Here, S denotes the factored form of two-mode squeezed operator $S(\tau)$, given by

$$S = \frac{1}{g} e^{-G a^\dagger b^\dagger} e^{-(a^\dagger a + b^\dagger b) \ln g} e^{G a b}, \quad (7)$$

where $G = \sqrt{g^2 - 1}/g$.

(iii) A conditional measurement, specifically the detection of a single-photon in the output idler mode, is represented by the projector $\Pi = |1\rangle_i\langle 1|$. A successful detection heralds the preparation of the output signal state:

$$|\psi_{out}\rangle = \mathcal{N} \Pi S |\phi\rangle_s |1\rangle_i, \quad (8)$$

where \mathcal{N} is a normalization constant. Note that in this protocol, the initial signal state $|\phi\rangle$ is arbitrary. From this perspective, the state generation protocol can be applied to any class of signal states. Following the derivation of Ref. [33], for a coherent state input $|\phi\rangle = |\alpha\rangle_s = D(\alpha)|0\rangle$, the unnormalized output state of the signal mode is given by:

$$|\psi_{out}\rangle \propto \left(\frac{1}{g^2} - \frac{G^2}{g} \alpha a^\dagger \right) |\alpha/g\rangle_s. \quad (9)$$

Here, $|\alpha/g\rangle_s$ represents an attenuated version of the initial signal state. Equation (9) is the central result of Ref. [33], showing that by tuning the amplitude gain g , one can generate specific nG states such as single-photon-added coherent states and displaced photon number states with high fidelity.

As previously noted, this protocol generalizes to non-coherent inputs. In the following sections, we demonstrate that using a SV state or a small-amplitude SC state as the signal input enables the generation of other useful nG states with extremely high fidelity.

III. SQUEEZED VACUUM SIGNAL INPUT

We now consider the case where the signal input is SV state, $|\phi\rangle_s = |\eta\rangle = S(\eta)|0\rangle$. Here, $S(\eta) = \exp[\frac{1}{2}(\eta^* a^2 -$

$\eta a^\dagger)^2)]$ is the single-mode squeezing operator with a complex squeezing parameter $\eta = re^{i\theta}$. The SV state $|\eta\rangle$ can be written in terms of Fock states as

$$|\eta\rangle = \frac{1}{\sqrt{\cosh r}} \sum_{n=0}^{\infty} e^{in\theta} (\tanh r)^n \frac{\sqrt{(2n)!}}{n! 2^n} |2n\rangle. \quad (10)$$

Following the protocol described in Sec. II, the unnormalized output state of the signal mode is determined by the conditional expression:

$$|\psi\rangle = \Pi S |\eta\rangle_a |1\rangle_b \\ = \Pi \frac{1}{g} e^{-G a^\dagger b^\dagger} e^{-(a^\dagger a + b^\dagger b) \ln g} e^{G a b} |\eta\rangle_a |1\rangle_b \quad (11)$$

To derive an explicit expression, we begin by applying the operator $e^{G a b}$ to the initial state:

$$|\psi'\rangle = e^{G a b} |\phi\rangle_a |1\rangle_b = (1 + G a b + \dots) |\phi\rangle_a |1\rangle_b \\ = |\phi\rangle_a |1\rangle_b + G a b |\phi\rangle_a |1\rangle_b \\ = |\phi\rangle_a |1\rangle_b - G e^{i\theta} \sinh r S(\eta) |1\rangle_a |0\rangle_b. \quad (12)$$

Next, we apply the operator $g^{-(a^\dagger a + b^\dagger b)}$ to $|\psi'\rangle$:

$$|\psi''\rangle = g^{-(a^\dagger a + b^\dagger b)} |\psi'\rangle \\ = \frac{1}{g} S(\eta) e^{-B \ln g} |0\rangle_a |1\rangle_b - G e^{i\theta} \sinh r S(\eta) e^{-B \ln g} |1\rangle_a |0\rangle_b, \quad (13)$$

where the operator B is defined as

$$B = a^\dagger a \cosh^2 r + a a^\dagger \sinh^2 r - \frac{e^{i\theta}}{2} a^{\dagger 2} \sinh 2r - \frac{e^{-i\theta}}{2} a^2 \sinh 2r. \quad (14)$$

We then apply the projector and the remaining exponential. The action of the projector on the first exponential term is:

$$\Pi e^{-G a^\dagger b^\dagger} = |1\rangle_{bb} \langle 1| (1 - G a^\dagger b^\dagger + \dots) \\ = |1\rangle_{bb} \langle 1| - G a^\dagger |1\rangle_{bb} \langle 0|. \quad (15)$$

Substituting the expressions, Eqs. (13) and (15) into the Eq. (11) yields the final unnormalized output state for the signal mode:

$$|\Psi\rangle = \frac{1}{g} \left[\frac{1}{g} S(\eta) e^{-B \ln g} |0\rangle_a + G^2 e^{i\theta} \sinh r a^\dagger S(\eta) e^{-B \ln g} |1\rangle_a \right]. \quad (16)$$

To simplify this expression, we must evaluate the action of $e^{-B \ln g}$ on the Fock states $|0\rangle_a$ and $|1\rangle_a$. We recognize that the operator B is an element of the $S(1, 1)$ Lie algebra. This allows us to factorize the exponential $e^{-B \ln g}$ into a disentangled form, which translates to a known sequence of squeezing and scaling operations on the vacuum state. To proceed, we define the generators

$$K_z = \frac{1}{2}(a^\dagger a + \frac{1}{2}), \quad (17)$$

$$K_+ = \frac{a^{\dagger 2}}{2}, \quad K_- = \frac{a^2}{2}, \quad (18)$$

which satisfy the $SU(1, 1)$ commutation relations [37]

$$[K_z, K_\pm] = \pm K_\pm, [K_+, K_-] = -2K_z. \quad (19)$$

Hence, we can write $e^{-B \ln g}$ as

$$A = e^{-B \ln g} = \lambda \exp \left[\frac{\phi_+(\theta')}{2} a^{\dagger 2} \right] \exp \left[\frac{\phi_z(\theta')}{2} a^\dagger a \right] \exp \left[\frac{\phi_-(\theta')}{2} a^2 \right], \quad (20)$$

where $\theta' = -\ln g$, $\alpha_\pm = -e^{\pm i\theta} \sinh 2r$, $\alpha_z = 2 \cosh 2r$, $\lambda = e^{\frac{1}{2}[\ln g + \phi_z(\theta')]} \sinh \Gamma \theta'$, and the coefficients ϕ_\pm , ϕ_z are given by

$$\Gamma = \sqrt{\frac{1}{4}\alpha_z^2 - \alpha_+ \alpha_-}, \quad (21a)$$

$$\phi_\pm(\theta') = \frac{\alpha_\pm}{\Gamma} \frac{\sinh \Gamma \theta'}{\cosh(\Gamma \theta') - \alpha_z \sinh(\Gamma \theta')/2\Gamma}, \quad (21b)$$

$$\phi_z(\theta') = -2 \ln \left[\cosh(\Gamma \theta') - \frac{\alpha_z}{2\Gamma} \sinh(\Gamma \theta') \right]. \quad (21c)$$

Applying this decomposition to the vacuum state is now simple, as the rightmost exponential annihilates it:

$$e^{-B \ln g} |0\rangle_a = \exp \left[\frac{\phi_+(\theta')}{2} a^{\dagger 2} \right] |0\rangle_a = \lambda \sqrt{\cosh r'} S(\xi) |0\rangle_a, \quad (22)$$

where $\xi = r' e^{i\varphi}$ and the real new squeezing parameter r' and phase φ are determined by $\phi_+(\theta') = -e^{i\varphi} \tanh r'$. This shows that the net effect on the vacuum is, up to a normalization, simply a squeezing operation. A similar, though more involved, calculation for the $|1\rangle_a$ state yields

$$e^{-B \ln g} |1\rangle_a = \lambda e^{\frac{\phi_z(\theta')}{2}} \exp \left[\frac{\phi_+(\theta')}{2} a^{\dagger 2} \right] |1\rangle_a = \lambda e^{\frac{\phi_z(\theta')}{2}} (\cosh r')^{\frac{3}{2}} S(\xi) |1\rangle_a. \quad (23)$$

In the above derivations, we used the Fock basis representation of the SV state, given in Eq. (10). Substituting these results back into the expression for $|\Psi\rangle$, the output state can be simplified to a compact form:

$$|\Psi'\rangle = \mathcal{N}'' S(\xi'') \left[c_0 |0\rangle + e^{2i\Theta(\eta, \xi)} c_2 |2\rangle \right], \quad (24)$$

where $\mathcal{N}'' = 1/\sqrt{|c_0|^2 + |c_2|^2}$ is the normalization constant and

$$c_0 = \frac{\lambda \sqrt{\cosh r'}}{g^2} - \frac{\lambda G^2}{g} e^{i\theta} \sinh r e^{\frac{\phi_z(\theta')}{2}} (\cosh r')^{\frac{3}{2}} \alpha_1, \quad (25)$$

$$c_2 = \sqrt{2} \frac{\lambda G^2}{g} \sinh r e^{\frac{\phi_z(\theta')}{2}} (\cosh r')^{\frac{3}{2}} \alpha_2 \quad (26)$$

with $\alpha_1 = \sinh r' \cosh r + \cosh r' \sinh r$, $\alpha_2 = \cosh r' \cosh r + \sinh r' \sinh r$, and $\xi'' = r'' e^{i\varphi''}$ defines the new squeezing parameter r'' and phase φ'' for the output state which determined by

$$\tanh r'' e^{i\varphi''} = \frac{\zeta_1 + \zeta_2}{1 + 2\zeta_1 \zeta_2^*} \quad (27)$$

with $\zeta_1 = \tanh r e^{i\theta}$, $\zeta_2 = \tanh r' e^{i\varphi}$, and the phase factor $\Theta(\eta, \xi)$ determined with

$$\Theta(\eta, \xi) = \frac{1}{i} \ln \left(\frac{1 + \zeta_1 \zeta_2^*}{1 + \zeta_1^* \zeta_2} \right). \quad (28)$$

This result indicates that the output state belongs to a family of squeezed superpositions of the zero- and two-photon Fock states. The coefficients of the superposition can be controlled by adjusting the initial squeezing parameter r and amplitude gain g . As shown in a recent study [38], such states are important resources for the efficient generation of high-fidelity, large-amplitude ($\alpha \geq 2$) SC states. Notably, this process is functionally equivalent to performing two-photon subtraction (a^2) from the original SV state, or to a sequence of single-photon-subtracted-and-added ($a^\dagger a$):

$$a^2 |r\rangle \propto S(r) \left[|0\rangle - \sqrt{2} \tanh r' |2\rangle \right], \quad (29)$$

$$a^\dagger a |r\rangle \propto S(r) \left[|0\rangle - \sqrt{2} (\tanh r')^{-1} |2\rangle \right], \quad (30)$$

where $|r\rangle = S(r) |0\rangle$ with real squeezing parameter r . The equivalence between these two operations can be verified through the relation

$$a^{\dagger 2} |r\rangle = -\coth r a^\dagger a |r\rangle. \quad (31)$$

To visualize the nG character of the output state, we numerically compute its Wigner function. As shown in Fig. 2, the Wigner functions of the input and output states are compared to illustrate the effects of the considered process. For the input signal states, panels (a) and (c) display the characteristic Gaussian profiles of SV states with squeezing parameters $r = 0.5$ and $r = 1.0$, respectively. The increased squeezing from (a) to (c) is evident as the Wigner function becomes more elongated along one quadrature. The corresponding output states, shown in panels (b) and (d) for a gain of $g = 2.5$, exhibit significant distortion and the emergence of pronounced negative regions (blue areas) in the phase space. These negative values are a direct signature of nonclassical properties, such as quantum interference, inherent to the output states. The clear structural change from a Gaussian input to a nG output underscores the strongly nonclassical nature of the resulting state.

As established in previous works [39], a squeezed superposition of the vacuum and two-photon Fock states can provide an excellent approximation to a large-amplitude squeezed even SC state, defined as

$$|\Psi_{sscs}\rangle = \mathcal{N}_{sscs} S(\gamma) [|\alpha\rangle + |-\alpha\rangle], \quad (32)$$

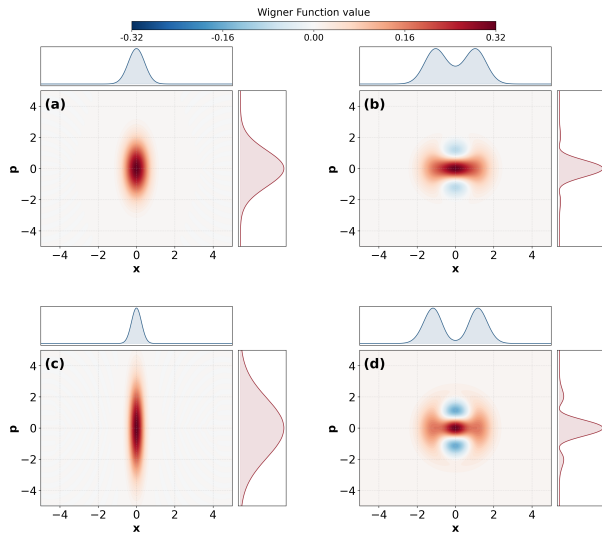


Figure 2. Wigner functions of the input and output states. (a) and (c) show the Wigner functions of the input SV states with squeezing parameters $r = 0.5$ and $r = 1.0$, respectively. The corresponding Wigner functions of the output signal states $|\Psi\rangle$ are shown in (b) and (d). The amplitude gain is fixed at $g = 2.5$.

where the normalization constant is $\mathcal{N}_{sscs} = (2 + 2e^{-2\alpha^2})^{-1/2}$. To quantify this, we numerically optimize the parameters γ and real amplitude α to maximize the fidelity $F = |\langle \Psi_{sscs} | \Psi \rangle|^2$ between the heralded state $|\Psi\rangle$ and an ideal squeezed even SC state. The fidelity is given by

$$F = \frac{4\nu e^{\frac{-2\alpha^2}{1+\nu^2}}}{1+\nu^2} \left| \chi \mathcal{N}_{sscs} \left(\sqrt{2} + \mu^* \frac{1 - \nu^4 + 4\nu^2\alpha^2}{(1+\nu^2)^2} \right) \right|^2, \quad (33)$$

where $\nu = e^{-(r'' - \gamma)}$, $\mu = \frac{c_2}{c_0}$, and $\chi = (1 + |\mu|^2)^{-\frac{1}{2}}$. In Fig. 3, we present the optimal fidelity between $|\Psi\rangle$ and $|\Psi_{sscs}\rangle$ as a function of the coherent amplitude α for fixed squeezing parameter $r'' = 1.0$. For each value of α in this plot, the squeezing parameter γ of the target state is optimized to maximize the fidelity with the generated state $|\Psi\rangle$. As shown in Fig. 3 for a fixed $r = 1.0$, the optimal fidelity reaches $F = 0.998$ at $\alpha \approx 1.38$, and $\gamma = 0.45$, indicating an extremely high degree of similarity between the generated state and the ideal squeezed even SC state. Previous studies have typically prepared the SC states using conditional heralding schemes based on photon subtraction from squeezed light [22, 23, 26, 32, 40]. A n -photon subtracted squeezed state $a^n S(\gamma) |0\rangle$, is a good approximation to certain squeezed SC states. For large n , the achievable amplitude of the SC state is at most $\alpha = \sqrt{n}$ [39]. The numerical data presented in Table I corroborate this finding.

Table I summarizes the optimized parameters and the corresponding fidelity between the output state generated under a fixed input SV state with $r = 1.0$ —and a

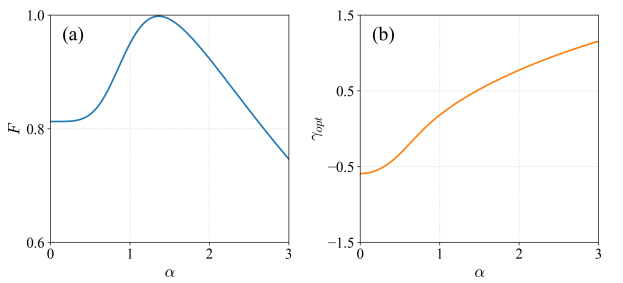


Figure 3. (a) Optimal fidelity between output state $|\Psi\rangle$ and the target squeezed even SC state. (b) Corresponding squeezing parameter γ of the target squeezed SC state that maximizes the fidelity in panel (a). The squeezing parameter of the initial SV state is fixed at $r = 1.0$. Other parameters are the same as in Fig. 2.

target squeezed even SC state, evaluated over a range of gain values g . When $g = 1.0$, the output state is identical to the input SV state. As g increases from 1.5 to 10.0, the optimal value of γ decreases, while the optimal α increases, saturating at approximately 1.4184 for $g \geq 5.0$. Notably, the fidelity remains high ($F \geq 0.997$) across the entire range of g , demonstrating the robustness and effectiveness of the protocol for generating the target nG state with extremely high fidelity. These results suggest that for a fixed r , the generated state converges to a squeezed even SC state with well-defined coherent amplitude, which becomes independent of g for sufficiently large gains. In other words, for an SV signal input, our protocol generates a squeezed even SC state $|\Psi_{sscs}\rangle$ with coherent amplitude $\alpha \approx \sqrt{2}$ and high fidelity. In this sense, our scheme with an SV input is equivalent to two-photon subtraction, $a^2 |\eta\rangle$, from the SV state [39, 41], achieving nearly perfect fidelity ($F = 0.999$). A key advantage of our scheme is that it generates the squeezed even SC state without explicitly performing two-photon subtraction.

Recent experimental works have demonstrated the generation of squeezed odd SC states with small ($\alpha < 1$) and larger ($\alpha \approx 1.4$) amplitudes using a continuous-wave low-loss waveguide OPA [42] and a conventional OPA [43], respectively. In both cases, an SV state is first prepared using an OPA. Subsequently, Ref. [42] employs the traditional scheme of a single-photon subtraction via an unbalanced beam splitter to generate a squeezed odd SC state with a fidelity of $F \approx 0.55$. In contrast, Ref. [43] uses a second OPA to generate a larger-amplitude squeezed odd SC state with a fidelity of $F \approx 0.61 \sim 0.65$. The key distinction of our model is that the OPA is not used directly as a source of squeezed light. Instead, it functions analogously to a beam splitter, primarily generating entanglement between the signal and idler modes. Furthermore, for an SV input, the heralding of a single photon in the idler output mode causes our scheme to effectively perform a continuous two-photon subtraction operation. Consequently, the output state is not a

g	γ	α	F
1.0	1.0	0	1
1.5	0.6158	1.2245	0.999
2.5	0.4470	1.3796	0.998
5.0	0.3689	1.4184	0.997
7.5	0.3500	1.4184	0.997
10.0	0.3440	1.4184	0.997

Table I. Optimized parameters for the fidelity between the generated state $|\Psi'\rangle$ and an ideal squeezed even cat state.

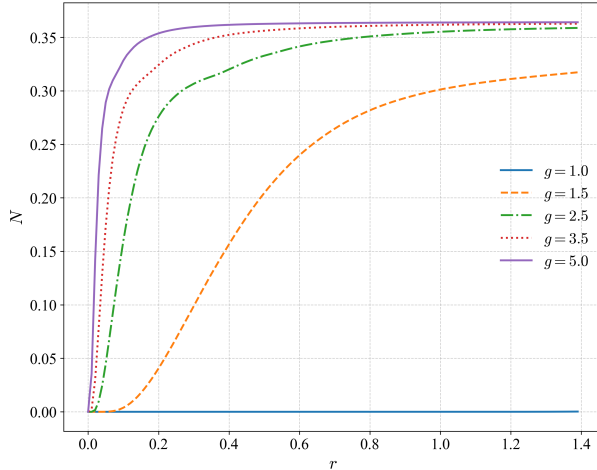


Figure 4. Dependence of the Wigner-negative volume N on the squeezing parameter r for different values of the amplitude gain g .

squeezed odd SC state, as in conventional schemes, but rather a squeezed even SC state with a larger coherent amplitude. Therefore, our model constitutes a new and feasible scheme for generating squeezed SC states with larger amplitudes and extremely high fidelity, outperforming traditional photon-subtraction methods.

To further quantify the overall extent of negativity in the Wigner distributions with changing the amplitude gain g , we use the Wigner-negative volume [44]. The Wigner-negative volume defined as:

$$N = \frac{1}{2} \int \int [|W(x, y)| - W(x, y)] dx dy. \quad (34)$$

Figure 4 shows the Wigner-negative volume N as a function of the squeezing parameter r for different values of the amplitude gain g . For $g = 1.0$ (blue solid line), the negativity volume N remains nearly zero for all r , consistent with the input SV state, which has a positive Wigner function. As the g increases, Wigner negativity emerges and becomes more pronounced. For any $g > 1$, the negativity volume N increases monotonically with the squeezing parameter r . Furthermore, for a fixed squeezing parameter r , a larger gain g yields a higher value of N , signifying a stronger nonclassical character in the generated state. The saturation of the curves at larger r indicates a limit on the achievable negativity volume for

a given g . The results in Table I and Fig. 4 demonstrate that the output state asymptotically approaches an even squeezed SC state with fixed parameters as the gain g and initial squeezing parameter r increase.

IV. SMALL-AMPLITUDE SC STATE SIGNAL INPUT

We now consider the case where the signal input is a small-amplitude SC state. These states are defined as

$$|\phi\rangle_\alpha = |SCS_\pm(\alpha)\rangle = \mathcal{N}_{\alpha\pm} (|\alpha\rangle \pm |-\alpha\rangle), \quad (35)$$

where the normalization constants are given by $\mathcal{N}_{\alpha\pm} = (2 \pm 2e^{-2\alpha^2})^{-1/2}$. SC states can be generated via several approaches, including photon subtraction from squeezed vacuum states [26] and cavity QED or circuit QED schemes [45, 46]. These techniques enable the preparation of optical and microwave SC states with controllable amplitudes, making them ideal testbeds for investigating nG quantum processes.

For the SC signal input states, the corresponding normalized output signal states is given by

$$\begin{aligned} |\Phi\rangle_\pm &= \mathcal{N} \left[\frac{1}{g^2} |\phi\rangle_{\alpha/g} - G^2 a^\dagger a |\phi\rangle_{\alpha/g} \right], \\ &= \mathcal{N}' \left[\frac{1}{g^2} \left(\left| \frac{\alpha}{g} \right\rangle \pm \left| -\frac{\alpha}{g} \right\rangle \right) - \frac{G^2 \alpha}{g} a^\dagger \left(\left| \frac{\alpha}{g} \right\rangle \mp \left| -\frac{\alpha}{g} \right\rangle \right) \right], \end{aligned} \quad (36)$$

where the normalization constant $\mathcal{N}' = \left[2(\beta^2 + G^4 |\frac{\alpha}{g}|^2) \right]^{-1/2}$ with $\beta = \frac{1}{g^2} - G^2 |\frac{\alpha}{g}|^2$. The output state is a superposition of the initial SC state and a photon-subtracted-and-added SC state. For larger amplitude gain g the second term which proportional to $a^\dagger a$ becomes dominant. While the photon number operator $a^\dagger a$ typically enlarges the state, the output amplitude in our protocol is attenuated by a factor of $\frac{\alpha}{g}$. This trade-off prevents amplitude enlargement, allowing the operation to primarily alter the state's nonclassicality.

If the gain is set to a critical value, $g = g_0 = \frac{1}{\sqrt{1-1/|\alpha|^2}}$, the output state simplifies to the following unnormalized

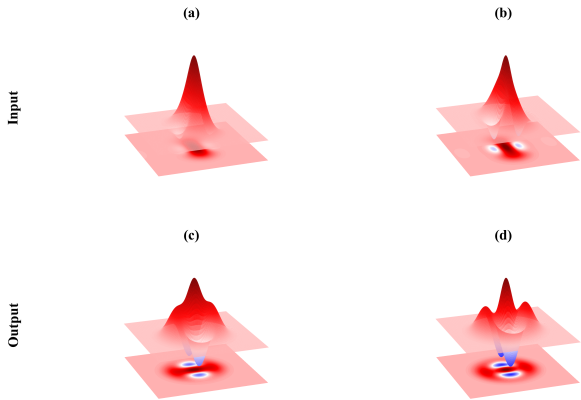


Figure 5. (a) and (b) show the Wigner functions of the input even SC state with coherent amplitudes $\alpha = 0.8$ and $\alpha = 1.01$, respectively. The corresponding Wigner functions of the output signal states are shown in (b) and (d), generated with amplitude gains $g = 5$ and $g = g_0$, respectively.

form:

$$\begin{aligned} |\Phi'\rangle_{\pm} &= -\frac{1}{\sqrt{2}} \left[D\left(\frac{\alpha}{g_0}\right) \mp D\left(-\frac{\alpha}{g_0}\right) \right] |1\rangle \\ &= \frac{g}{\sqrt{2}\alpha} \mathcal{N}_{\alpha/g_0, \pm}^{-1} \left(\frac{|\alpha|^2}{g_0^2} - a^\dagger a \right) |\phi\rangle_{\alpha/g_0}. \end{aligned} \quad (37)$$

In this case, the output corresponds to a superposition of displaced number states.

Figure 5 shows the Wigner function distributions of the input even SC states and their corresponding output states. Panels (a) and (b) present the Wigner functions of the input even SC states with coherent amplitudes $\alpha = 0.8$ and $\alpha = 1.01$, respectively. Due to the relatively small coherent amplitudes, both input states exhibit nearly Gaussian profiles, lacking pronounced nG features or significant negative regions. In contrast, panel (c) shows the output state for the input in (a) with a gain $g = 5$. A distinct negative region emerges, indicating a considerable enhancement of non-Gaussianity. This trend is more pronounced in panel (d), which shows the output for input from (b) at the critical gain $g = g_0$. The state exhibits broader and deeper negative regions, confirming the effective amplification of non-Gaussianity. Furthermore, for the $g = g_0$ and $\alpha = 1.01$ [see Fig. 5 (d)], the generated state has an extremely high fidelity ($F > 0.999$) with the state $|\phi_2\rangle = |0\rangle - 1.416|2\rangle$.

The origin of this specific state can be explained as follows. For $g = g_0$ and $\alpha = 1.01$ (giving $\alpha/g_0 = 0.142$), the output state in Eq. (34) becomes $0.02|\phi\rangle_{0.142} - 0.98a^\dagger a|\phi\rangle_{0.142}$ (unnormalized), where $|\phi\rangle_{0.142} = |SCS_+(0.142)\rangle$ is the even SC state with amplitude $\alpha = 0.142$. An even SC state with $\alpha \lesssim 0.75$ closely resembles ($F > 0.99$) a Gaussian SV state [47]. Consequently, the output state is equivalent to $0.02S(r_{opt})|0\rangle - 0.98a^\dagger aS(r_{opt})|0\rangle$ where r_{opt} is the squeezing parameter that optimizes the fidelity and de-

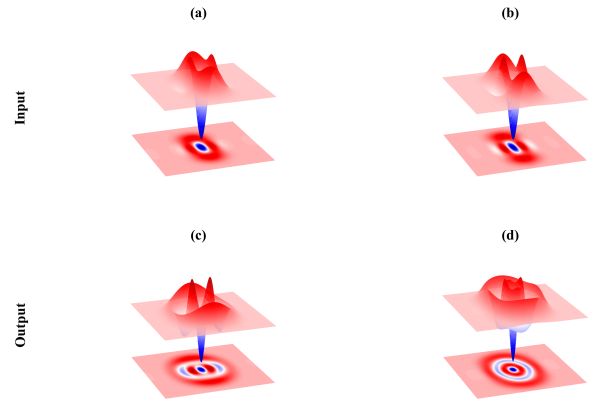


Figure 6. (a) and (b) show the Wigner functions of the input odd SC state with coherent amplitudes $\alpha = 1.2$ and $\alpha = 1.5$, respectively. The corresponding Wigner functions of the output signal states are shown in (c) and (d), obtained with amplitude gains of $g = 1.5$ and $g = g_0$, respectively.

pends on α . Using the relations in Eqs. (29-31) and choosing an optimized r_{opt} (≈ 0) yields the state $|\phi_2\rangle$.

Figure 6 illustrates the evolution of the Wigner functions when an odd SC state with small coherent amplitude is used as the input. Panels (a) and (b) show the Wigner functions of the input odd SC states with coherent amplitudes $\alpha = 1.2$ and $\alpha = 1.5$, respectively. These states are characterized by a deep negative dip at the origin of phase space, reflecting the odd parity of their wavefunctions. The corresponding output states, obtained with gains $g = 1.5$ panel (c) and $g = g_0$ panel (d), exhibit pronounced structural changes. In particular, the output state in panel (d), generated at the critical gain, develops intricate ring-like patterns and closely approximates a squeezed three-photon number state, $\frac{1}{\sqrt{6}}S(r)a^\dagger a^3|0\rangle$, with a fidelity exceeding 0.99 for an optimal squeezing parameter $r = -0.23$. The emergence of this squeezed three-photon state can be explained as follows. In the small-amplitude regime ($\alpha \leq 1.2$), an odd SC state is well approximated by a squeezed single-photon state, $S(r_{opt}')|1\rangle = \frac{1}{\cosh r_{opt}'}a^\dagger S(r_{opt}')|0\rangle$, with a fidelity exceeding 0.99 [26]. The odd SC state with amplitude $\alpha/g_0 = 1.12$ in Eq. (34) can be approximated by $a^\dagger S(r_{opt}')|0\rangle$. Subsequent calculation shows that the output then approximates $\frac{1}{\sqrt{6}}S(r_{opt}')a^\dagger a^3|0\rangle$, with $r_{opt}' = -0.23$.

Conventional methods for generating photon-number states typically involve producing a TMSV state from a nonlinear crystal (e.g., BBO) and performing photon-number-resolving detection (PNRD) on the idler mode using a visible-light photon counter (VLPC) [48]. A successful detection of n photons in the idler arm heralds the preparation of the photon-number state $|n\rangle$ in the signal mode. However, such schemes impose stringent requirements on the detector: current PNRDs cannot reliably resolve large photon numbers, and their detection

efficiency deteriorates significantly as n increases. In contrast, our scheme—using an odd SC state as an input—requires the detection of only a single photon in the idler mode to herald the generation of an approximate three-photon Fock state in the signal mode. Thus, our protocol provides a resource-efficient method for generating specific photon-number states, circumventing the need for high-performance PNRDs. This approach is readily scalable and adaptable to a broad range of quantum optical platforms. Although the resulting state exhibits a small degree of squeezing, this can be compensated for with an additional OPA stage. Consequently, the resulting (squeezed) three-photon state has potential applications in quantum error correction [49, 50], quantum channel capacity optimization [51, 52], and quantum phase estimation [53, 54]. In previous work [43], sequential usage of OPA implements a single-mode squeezing operation to generate small amplitude SC states heralded with single-photon subtraction with the aim of additional beam splitter first and amplify it. In contrast, our heralding scheme uses the OPA differently; its overall effect is not to amplify the initial SC state but to significantly enhance its non-Gaussianity.

To further investigate the effect of the OPA on input SC states, we plot the Wigner-negative volume N as a function of state amplitude α for different amplitude gains g , as shown in Fig. 7. Figure 7 (a) shows the results for an even SC state input. The negativity N_+ increases monotonically with α for all amplitude gains g , eventually saturating at larger amplitudes. For all $g > 1$, the value of N_+ is greater than that of the initial state ($g = 1$), demonstrating the effectiveness of the OPA in enhancing the non-Gaussianity of the even SC state. In contrast, Fig. 7 (b) presents the case of an odd SC state input, where N_- exhibits a non-monotonic dependence on α for different amplitude gains g . The negativity first reaches a maximum for an intermediate gain (e.g., $g = 1.4$) and then decreases as g increases further.

These behaviors can be understood from the form of the output state in Eq. (36). For an even SC input, the nG character of the output state is dominated by the term $\frac{G^2\alpha}{g}a^\dagger\left(\left|\frac{\alpha}{g}\right\rangle - \left|-\frac{\alpha}{g}\right\rangle\right)$, whose relative weight increases with g . Since this component resembles an odd SC state, it retains significant nonclassicality even in the limit $\frac{\alpha}{g} \rightarrow 0$. Consequently, N_+ grows with α and eventually saturates. In contrast, for an odd SC input, the dominant nG component is $\frac{G^2\alpha}{g}a^\dagger\left(\left|\frac{\alpha}{g}\right\rangle + \left|-\frac{\alpha}{g}\right\rangle\right)$. However, as g increases and $\frac{\alpha}{g} \rightarrow 0$, the contribution of this term diminishes, leading to a reduction in nonclassicality. This explains the non-monotonic, rise-and-fall behavior of N_- as a function of α for different amplitude gains g .

In summary, the numerical analysis confirms that the proposed protocol can effectively manipulate and enhance the non-Gaussianity of both even and odd SC states.

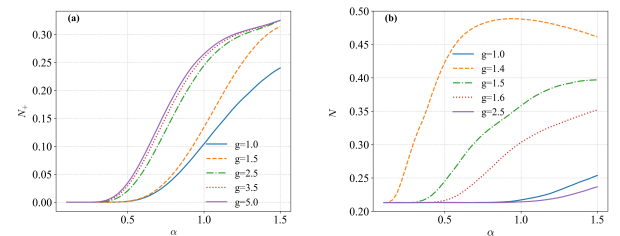


Figure 7. Dependence of the Wigner-negative volume N on the coherent state amplitude α for different values of the amplitude gain g .

V. INFLUENCE OF PHOTO LOSS

From a practical perspective, it is essential to analyze the decoherence of the generated quantum states due to photon loss. When a quantum state is coupled to an environment, it typically undergoes a transition from non-Gaussian to Gaussian characteristics. In a photon-loss channel, the negative regions of the Wigner function—a hallmark of non-Gaussianity—gradually disappear. The evolution of the density matrix ρ , which quantitatively describes this dynamical behavior, can be modeled using the Lindblad–Gorini–Kossakowski–Sudarshan (LGKS) master equation [55]:

$$\frac{d\rho}{dt} = \kappa (2apa^\dagger - a^\dagger a\rho - \rho a^\dagger a),$$

where κ is the decay rate, and the dimensionless time κt characterizes the dissipation strength. The decoherence dynamics are illustrated in Fig. 8, which shows the Wigner functions of the output states obtained by numerically solving the LGKS master equation for different values of κt . The blue regions, representing negative Wigner function values, gradually shrink and eventually vanish as κt increases. Furthermore, the separation between the two peaks in the cat-like states decreases, eventually merging into a single Gaussian peak. This behavior indicates that the initial nG states progressively lose their nonclassicality and non-Gaussianity through interaction with the environment, eventually decaying into Gaussian states.

VI. DISCUSSION AND CONCLUSION

In this work, we have generalized the heralded OPA protocol into a highly versatile and practical source for distinct classes of nG states. By moving beyond the coherent state inputs of previous scheme, we have demonstrated that a single, integrated setup can perform two critical functions: the generation of high-fidelity, larger-amplitude squeezed SC states from a SV input, and the significant amplification of non-Gaussianity from small-amplitude SC states, producing tailored photon number superpositions.

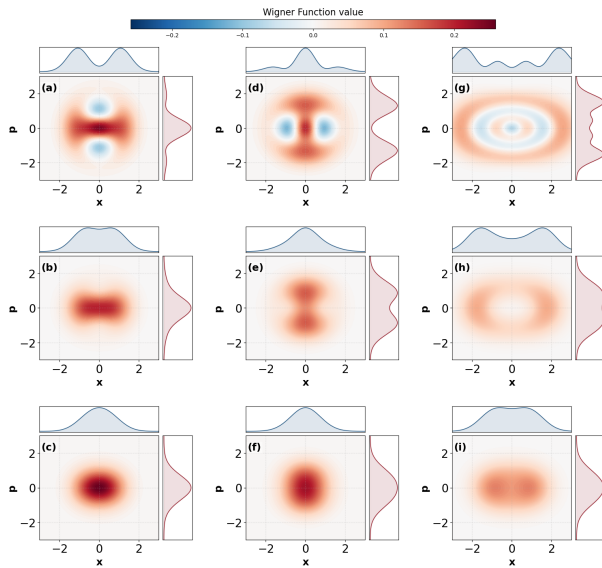


Figure 8. Wigner functions of the output states under different dissipation strengths. Panels (a)-(c) show the SV input state with $r = 1.0$ and $g = 2.5$; (d)-(f) display the even SC state ($\alpha = 1.2$, $g = g_0$); and (g)-(i) present the odd SC state ($\alpha = 1.5$, $g = g_0$). Each row corresponds to different rescaled time $\kappa t = 0.1, 0.5, 1.0$, respectively.

A key finding of our analysis is the protocol’s intrinsic equivalence to an integrated two-photon subtraction for a SV input. This operation is achieved not with discrete, lossy optical components, but within the stable environment of the OPA itself, yielding a squeezed even SC state with a coherent amplitude of $\alpha \approx 1.4$ —a value challenging to achieve with sequential single-photon subtraction. Furthermore, when the input is a small-amplitude SC state, the protocol acts as a non-Gaussianity engine, distilling states that closely approximate high-value

resources—such as the specific superposition $|0\rangle - 1.4|2\rangle$ and squeezed three-photon state—with fidelities exceeding 0.99. The robustness of these states is confirmed by their retention of significant Wigner negativity under initial, realistic levels of photon loss, underscoring their potential for practical applications.

The experimental viability of our proposal is firmly supported by its practical performance metrics. The calculated per-trial success probabilities, ranging from 10^{-4} to 10^{-2} for a gain $g \in [1, 10]$, are commensurate with other established heralding schemes including SPAC states [20] and cluster state generation [5]. When combined with modern high-repetition-rate laser sources [32, 56, 57], these probabilities translate to substantial absolute generation rates of 10^5 to 10^7 states per second, confirming the experimental feasibility of our proposal.

The performance and scalability of this protocol are poised for further enhancement through technological advances. Progress in low-loss integrated photonics [58] will minimize decoherence, while advances in high-efficiency superconducting single-photon detectors [59, 60] will maximize the heralding efficiency and thus the effective generation rate. The inherent versatility and integrated nature of our scheme make it highly amenable to these ongoing developments.

In summary, this work significantly expands the toolbox for quantum state engineering by providing a unified, flexible, and experimentally accessible platform for generating high-purity nG states. The heralded OPA protocol thus constitutes a promising and versatile workhorse for advancing CV quantum computation, metrology, and other related information processing.

ACKNOWLEDGMENTS

This study was supported by the National Natural Science Foundation of China (No. 12365005).

[1] M. Walschaers, *PRX Quantum* **2**, 030204 (2021).

[2] M. Walschaers, V. Parigi, and N. Treps, *PRX Quantum* **1**, 020305 (2020).

[3] S. Lloyd and S. L. Braunstein, *Phys. Rev. Lett.* **82**, 1784 (1999).

[4] D. Gottesman, A. Kitaev, and J. Preskill, *Phys. Rev. A* **64**, 012310 (2001).

[5] N. C. Menicucci, P. van Loock, M. Gu, C. Weedbrook, T. C. Ralph, and M. A. Nielsen, *Phys. Rev. Lett.* **97**, 110501 (2006).

[6] K. Miyata, H. Ogawa, P. Marek, R. Filip, H. Yonezawa, J.-i. Yoshikawa, and A. Furusawa, *Phys. Rev. A* **93**, 022301 (2016).

[7] A. Mari and J. Eisert, *Phys. Rev. Lett.* **109**, 230503 (2012).

[8] K. Fukui, A. Tomita, A. Okamoto, and K. Fujii, *Phys. Rev. X* **8**, 021054 (2018).

[9] P. M. Anisimov, G. M. Raterman, A. Chiruvelli, W. N. Plick, S. D. Huver, H. Lee, and J. P. Dowling, *Phys. Rev. Lett.* **104**, 103602 (2010).

[10] S. D. Huver, C. F. Wildfeuer, and J. P. Dowling, *Phys. Rev. A* **78**, 063828 (2008).

[11] G. S. Agarwal and K. Tara, *Phys. Rev. A* **43**, 492 (1991).

[12] M. S. Kim, F. A. M. de Oliveira, and P. L. Knight, *Phys. Rev. A* **40**, 2494 (1989).

[13] L. Duan, *Nat. Photonics* **13**, 73 (2019).

[14] B. Yurke and D. Stoler, *Phys. Rev. Lett.* **57**, 13 (1986).

[15] C. C. Gerry, *Phys. Rev. A* **55**, 2478 (1997).

[16] V. Parigi, A. Zavatta, M. Kim, and M. Bellini, *Science* **317**, 1890 (2007).

[17] A. I. Lvovsky and J. Mlynek, *Phys. Rev. Lett.* **88**, 250401 (2002).

[18] Q. Hu, T. Yusufu, and Y. Turek, *Phys. Rev. A* **105**, 022608 (2022).

[19] X.-X. Yao and Y. Turek, “Non-gaussian state preparation and enhancement using weak-value amplification,”

(2025), arXiv:2506.14632 [quant-ph].

[20] A. Zavatta, S. Viciani, and M. Bellini, *Science* **306**, 660 (2004).

[21] J. Wenger, R. Tualle-Brouri, and P. Grangier, *Phys. Rev. Lett.* **92**, 153601 (2004).

[22] K. Wakui, H. Takahashi, A. Furusawa, and M. Sasaki, *Opt. Express* **15**, 3568 (2007).

[23] J. S. Neergaard-Nielsen, B. M. Nielsen, C. Hettich, K. Mølmer, and E. S. Polzik, *Phys. Rev. Lett.* **97**, 083604 (2006).

[24] M. Barbieri, N. Spagnolo, M. G. Genoni, F. Ferreyrol, R. Blandino, M. G. A. Paris, P. Grangier, and R. Tualle-Brouri, *Phys. Rev. A* **82**, 063833 (2010).

[25] Y.-R. Chen, H.-Y. Hsieh, J. Ning, H.-C. Wu, H. L. Chen, Z.-H. Shi, P. Yang, O. Steuernagel, C.-M. Wu, and R.-K. Lee, *Phys. Rev. A* **110**, 023703 (2024).

[26] A. Ourjoumtsev, R. Tualle-Brouri, J. Laurat, and P. Grangier, *Science* **312**, 83 (2006).

[27] S. J. van Enk and O. Hirota, *Phys. Rev. A* **64**, 022313 (2001).

[28] S. L. Braunstein and P. van Loock, *Rev. Mod. Phys.* **77**, 513 (2005).

[29] Y. Guo, W. Ye, H. Zhong, and Q. Liao, *Phys. Rev. A* **99**, 032327 (2019).

[30] M. Walschaers, B. Sundar, N. Treps, L. D. Carr, and V. Parigi, *Quantum Sci. Technol.* **8**, 035009 (2023).

[31] A. Ourjoumtsev, H. Jeong, R. Tualle-Brouri, and P. Grangier, *Nature* **448**, 784 (2007).

[32] K. Takase, J.-i. Yoshikawa, W. Asavanant, M. Endo, and A. Furusawa, *Phys. Rev. A* **103**, 013710 (2021).

[33] S. U. Shringarpure and J. D. Franson, *Phys. Rev. A* **100**, 043802 (2019).

[34] B. L. Schumaker and C. M. Caves, *Phys. Rev. A* **31**, 3093 (1985).

[35] C. M. Caves, J. Combes, Z. Jiang, and S. Pandey, *Phys. Rev. A* **86**, 063802 (2012).

[36] H. A. Haus and J. A. Mullen, *Phys. Rev.* **128**, 2407 (1962).

[37] R. R. Puri *et al.*, *Mathematical methods of quantum optics*, Vol. 79 (Springer, 2001).

[38] H. Luo and S. Mahmoodian, “Efficient optical cat state generation using squeezed few-photon superposition states,” (2024), arXiv:2412.14798 [quant-ph].

[39] P. Marek, H. Jeong, and M. S. Kim, *Phys. Rev. A* **78**, 063811 (2008).

[40] M. Dakna, T. Anhut, T. Opatrný, L. Knöll, and D.-G. Welsch, *Phys. Rev. A* **55**, 3184 (1997).

[41] M. Takeoka, H. Takahashi, and M. Sasaki, *Phys. Rev. A* **77**, 062315 (2008).

[42] K. Takase *et al.*, *Opt. Express* **30**, 14161 (2022).

[43] M. Wang, M. Zhang, Z. Qin, Q. Zhang, L. Zeng, X. Su, C. Xie, and K. Peng, *Laser Photonics Rev.* **16**, 2200336 (2022).

[44] A. Kenfack and K. Życzkowski, *J Opt B Quantum Semiclassical Opt* **6**, 396 (2004).

[45] J.-Q. Liao, J.-F. Huang, and L. Tian, *Phys. Rev. A* **93**, 033853 (2016).

[46] Z. Zhang, L. Shao, W. Lu, and X. Wang, *Phys. Rev. A* **106**, 043721 (2022).

[47] A. M. Brańczyk and T. C. Ralph, *Phys. Rev. A* **78**, 052304 (2008).

[48] E. Waks, E. Diamanti, and Y. Yamamoto, *New J. Phys.* **8**, 4 (2006).

[49] E. Knill and R. Laflamme, *Phys. Rev. A* **55**, 900 (1997).

[50] S. B. Korolev, E. N. Bashmakova, and T. Y. Golubeva, *Quantum Inf. Process.* **23**, 354 (2024).

[51] Y. Yamamoto and H. A. Haus, *Rev. Mod. Phys.* **58**, 1001 (1986).

[52] C. M. Caves and P. D. Drummond, *Rev. Mod. Phys.* **66**, 481 (1994).

[53] P. Najafi, G. Naeimi, and S. Saeidian, *Sci. Rep.* **13**, 15268 (2023).

[54] L. T. Knoll, A. G. Magnoni, and M. A. Larotonda, *Entropy* **27** (2025), 10.3390/e27070712.

[55] H.-P. Breuer and F. Petruccione, *The theory of open quantum systems* (OUP Oxford, 2002).

[56] K. Wakui, Y. Tsujimoto, M. Fujiwara, I. Morohashi, T. Kishimoto, F. China, M. Yabuno, S. Miki, H. Terai, M. Sasaki, and M. Takeoka, *Opt. Express* **28**, 22399 (2020).

[57] H. Chen, Z. You, and K. Xu, *Opt. Laser. Technol.* **181**, 111703 (2025).

[58] R. Chen, Y.-H. Luo, J. Long, B. Shi, C. Shen, and J. Liu, *Phys. Rev. Lett.* **133**, 083803 (2024).

[59] W. H. P. Pernice, C. Schuck, O. Minaeva, M. Li, G. N. Goltzman, A. V. Sergienko, and H. X. Tang, *Nat. Commun.* **3**, 1325 (2012).

[60] B. Korzh *et al.*, *Nat. Photonics* **14**, 250 (2020).